

Numerical simulations for description of UV laser interaction with gold nanoparticles embedded in silica

F. BONNEAU^{1,✉}
P. COMBIS¹
J.L. RULLIER¹
J. VIERNE¹
B. BERTUSSI²
M. COMMANDRÉ²
L. GALLAIS²
J.Y. NATOLI²
I. BERTRON³
F. MALAISE³
J.T. DONOHUE⁴

¹ Département de Physique Théorique et Appliquée, CEA/DAM Ile de France, BP12, 91680 Bruyères le Châtel, France

² Institut Fresnel, Domaine Universitaire de St Jérôme, 13397 Marseille, France

³ Département d'Etude et Validation, CEA/Centre d'Etudes Scientifiques et Techniques d'Aquitaine, BP 2, 33114 Le Barp, France

⁴ Centre d'Etudes Nucléaires de Bordeaux-Gradignan, BP 120, 33175 Gradignan, France

Received: 7 August 2003/Final version: 21 November 2003
Published online: 3 February 2004 • © Springer-Verlag 2004

ABSTRACT We have performed simulations of laser energy deposition in an engineered absorbing defect (i.e. metal nanoparticle) and the surrounding fused silica taking into account various mechanisms for the defect-induced absorption of laser energy by SiO₂. Then, to simulate the damage process in its entirety, we have interfaced these calculations of the energy absorption with a 2-D Lagrange–Euler hydrodynamics code, which can simulate crack formation and propagation leading to craters. The validation of numerical simulations requires detailed knowledge of the different parameters involved in the interaction. To concentrate on a simple situation, we have made and tested a thin-film system based on calibrated gold nanoparticles (600-nm diameter) inserted between two silica layers. Some aspects of our simulations are then compared with our experimental results. We find reasonable agreement between the observed and simulated crater sizes.

PACS 61.80.Ba; 42.70.-a; 52.38.Mf

1 Introduction

In order to advance our understanding of laser-induced damage in optical glass (fused silica), it is necessary to confront experimental results with simulations. At fluxes of 10¹⁰ W/cm², damage initiation is not deterministic, but is rather linked to the presence of surface or sub-surface defects in the silica [1–4]. Phase transitions and plasma formation caused by laser absorption in defects may induce shocks in the surrounding silica. Failure and fractures of the silica may then occur, depending on the particular experimental conditions: fluence and pulse shape of the laser, type of defect, diameter and depth of the defect. The history or conditioning of the sample may also influence failure and fracture events. In powerful laser devices, defects, either superficial or embedded not too deeply, may absorb laser energy and expand violently, leading to the formation of craters on the surface. The diameter of these craters may range from 1 to 100 μm, depending both on the size of the defect and its depth. The distribution of craters on an optical surface after a laser shot is random [5–7]

and is correlated with a defect distribution which is at present undetectable before the laser irradiation. In order to investigate the damage phenomenology, calibrated targets, in which inclusions of definite size and composition are embedded in ultra-pure silica at a well-known depth, have been studied by several groups [8–11].

The failure scenario of glass by laser illumination of metallic inclusions essentially involves two distinct physical processes: first the deposit of radiant energy in the inclusion, which causes the expansion of the inclusion, leading to both compressive and tensile stresses in the surrounding glass matrix. When these compressive or tensile stresses exceed, respectively, the fragmentation and the fracture limits of the glass, the second process, fragmentation or crack formation, will occur. While this seems to be a straightforward problem, it involves electrodynamics, thermodynamics and mechanics of continuous media. In addition, there are external constraints imposed by the duration of the laser pulse, a few nanoseconds in our case, and its typical fluence, a few J/cm². The time scales for the thermal relaxation and mechanical deformation of both the inclusion and the surrounding silica are typically shorter than nanoseconds, so it becomes necessary to study the problem in a time-dependent way during the laser pulse. The size, density and temperature of the inclusion change with time, causing the deposit of energy by the laser to be time dependent as well. Melting or even boiling of the metal may also occur. Heat can be transferred from the inclusion to the surrounding glass by both conduction and radiation, possibly leading to the formation of a dense plasma, which can itself absorb energy from the laser [12]. The aim of the modeling is to take into account the main effects, using as much of the available knowledge as possible on the electrical, thermal and mechanical properties of the two media. We address this problem with the help of two codes, one 1-D (called DELPOR) principally designed to describe the deposit of energy in the inclusion, and the other 2-D (called HESIONE) which is used to study the initiation and growth of cracks in the surrounding silica. These are proprietary codes of the Commissariat à l'Energie Atomique. The former is in FORTRAN, and typical running times are a few minutes on 1-GHz processors. The latter includes both FORTRAN and C components, and typical runs require a few hours.

✉ Fax: +33-1/69267106, E-mail: florian.bonneau@cea.fr

With the aim to evaluate the modeling approach, we study engineered samples in which calibrated gold defects are embedded in pure thin films of deposited silica. We used gold spheres with diameters of order 600 nm, which are much larger than inclusions used in previous studies [10, 11]. It is clear that real damage-inducing inclusions are much smaller than these spheres [13], but the physics used in our codes should be valid at this scale, making it a good place to validate the codes before proceeding to simulations of smaller inclusions. Moreover, by using such a large sphere, we can locate its position and observe it (with an optical microscope) both before and after the laser shot. This allows us to make a comparison with simulations.

This article is organized as follows: in Sect. 2 we briefly describe the codes DELPOR and HESIONE used to perform the simulations, and the main results are discussed in Sect. 3. Our experiments on these engineered defect-bearing samples are related in Sect. 4, and the results are compared with numerical simulations.

2 Description of simulations

To numerically represent the interaction between the laser beam and the metallic sphere surrounded by silica we used a 1-D hydrodynamic Lagrangian code [11] (called DELPOR). In Fig. 1a we show an illustration of the problem that is treated by DELPOR, that of a spherical inclusion in a larger silica sphere. In this code, the laser energy deposition is determined by solving the Helmholtz electromag-

netic equation [14]. To take into account the laser absorption in a spherical nanoparticle and the surrounding ionized silica, we use the code in spherical geometry and we solve the Helmholtz equation thanks to the Mie theory [15, 16], generalized to media where the indices of refraction may depend continuously on the radius [17]. The electric field amplification in the silica close to the particle can induce local ionization, which involves laser absorption in initially transparent silica [18]. The electromagnetic fields and the deposit of energy in the inclusion are calculated in a fully 3-D manner. However, the energy input to our 1-D code at a given interval in radius is in fact the integral of the electromagnetic energy density deposited in the corresponding spherical shell. The DELPOR code can simulate ionization and induced absorption of the surrounding silica with effective frequencies and ionization frequencies obtained by means of a specific Monte Carlo calculation program [19]. Thermal conduction, radiative transfer, ionization by UV light emitted by the hot metallic particle and the mechanical propagation of shock waves are also simulated in DELPOR. These simulations need accurate data such as multi-phase equations of state [20] and transport coefficients in solids, liquids, vapors and dense or diluted plasmas (refractive indices [21], electric and thermal conductivities [22, 23], opacities, collision and ionization frequencies [24], multi-photon ionization coefficients [25], . . .) and mechanical properties (material strengths, . . .).

The problem of a gold inclusion embedded in a thin-film silica matrix irradiated by a laser is depicted schematically in Fig. 1b. Gold spheres, of diameter 600 nm, are deposited and covered by a film of silica. The laser pulse is incident on the air–silica film interface as shown in the figure. The effect of the dome, which results from the deposit of silica, is included in the simulation, and the silica matrix is assumed to be uniform throughout the sample. To resolve this problem of mechanical effects of a gold inclusion in the silica matrix, DELPOR can be used at each time as the preprocessor of our hydrodynamics code HESIONE which includes brittle fracture. HESIONE is a 2-D code (assuming axial symmetry), which means that it predicts fracture lines that are in fact surfaces of revolution. It combines both a Lagrangian (with mesh attached to the moving media) and an Eulerian (fixed-frame) description, passing from one description to the other as needed. We use a damage model to describe the effects of cracking (damage occurring in silica under tensile stresses) and for what we call fragmentation (damage occurring in silica under compressive stresses) in the framework of the mechanics of continuous media. The medium is represented by a discrete set of lattice points. At each point, the model allows the formation of up to three orthogonal fracture surfaces, characterizing the fracture triad. The formation of these fracture surfaces involves tensile failure, when a tensile stress applied perpendicularly to one of these fracture surfaces exceeds the dynamic tensile strength of glass (0.5 GPa). The formation of a fracture surface is also accompanied by the relaxation of the stress vector, which is perpendicular to this surface. We use the model proposed by Rubin and Attia [26, 27] to represent the effects of oriented cracking. Another source of damage is fragmentation, which occurs when the silica is subjected to very high compressive stresses (3 GPa). We defined the

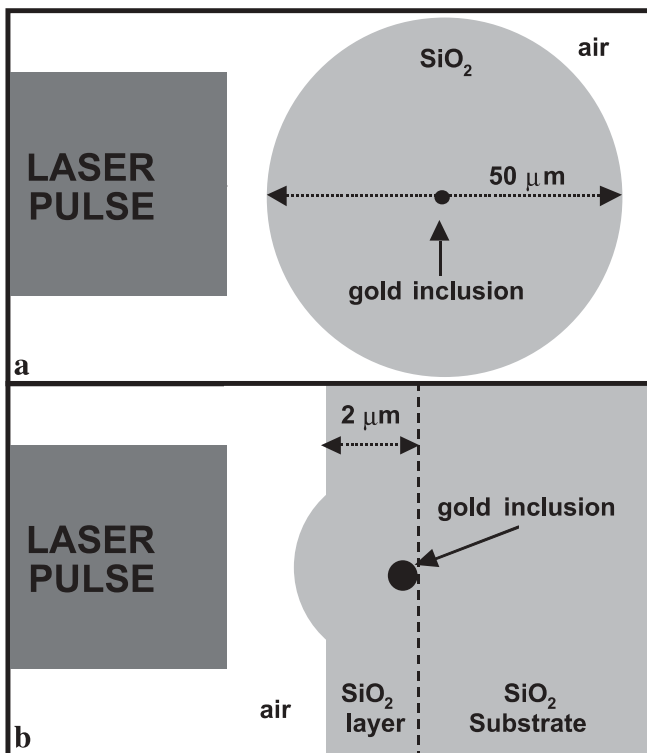


FIGURE 1 Configurations of two different geometries studied in this work, both with gold spheres of 600-nm diameter: **a** the inclusion is embedded in a spherical bulk silica substrate, **b** the inclusion is deposited on a thin silica film deposited on a bulk silica substrate, and is then covered by a second silica thin film

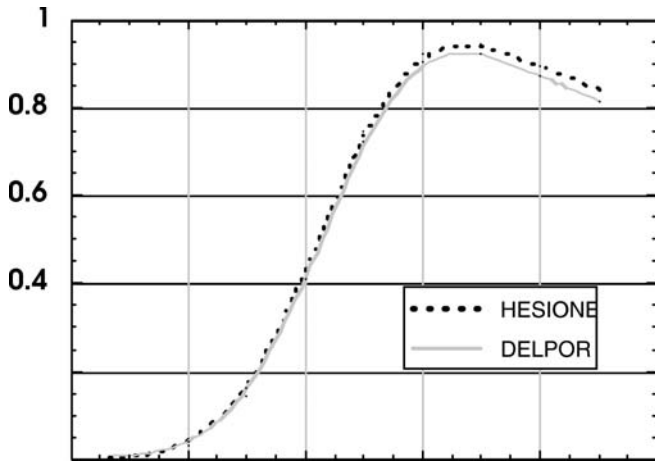


FIGURE 2 The pressure in the gold inclusion as a function of time t in the laser pulse, as calculated by the 1-D code DELPOR (solid curve) and the 2-D code HESIONE (dashed curve), for a fluence of 0.1 J/cm^2

threshold for plastic flow as a function of both the mean stress and the fragmentation intensity. A scalar damage variable D is defined in order to quantify the fragmentation intensity. It ranges from 0 (undamaged) to 1 (fully damaged). During the simulation its value as a function of space and time depends on the deformation tensor at the same point. The shear modulus and the yield strength are parameterized as linear functions of D .

Our major innovation consists in interfacing these two codes in order to treat the damage problem in its entirety. At each time step, the space-time evolution of internal energy in the inclusion and the surrounding silica as obtained with DELPOR is injected into HESIONE, which then calculates the evolution of the two media. This process is repeated throughout the pulse. The presence of the free surface leads to reflection and interaction of the shock waves, which play a very important role in generating and propagating cracks. In order to assure some measure of consistency between the two codes, we impose the following conditions.

1. The same initial temperature and density at time $t = 0$.
2. The same equations of state are used in both codes (multi-phase for the inclusion and Mie-Grüneisen for the silica).
3. Both codes use the same constitutive relationships for silica. For this, we have to implement the shear modulus μ and the elastic limit Y as functions of the internal energy density E . (When the melting temperature is reached, $\mu(E)$ and $Y(E)$ vanish.)

Although imposing these conditions is essential to making our results roughly self-consistent, there are intrinsic differences between the two codes. The first is the dimension (1-D and 2D), and another is the capacity for HESIONE to correctly treat fissure formation and fragmentation in the silica. In order to illustrate the consistency, we show in Fig. 2 the pressure (in the inclusion) as a function of time, according to the codes DELPOR (solid curve) and HESIONE (dashed curve) for a fluence of 0.1 J/cm^2 . Both curves are quite similar. At this low fluence, no significant cracking occurs, and the pressures calculated inside the inclusion by the two codes are in good accordance. However, at higher fluence, the capability to represent the effects of cracking and fragmentation means the pressure is no longer isotropic in the inclusion and does not attain the same level as that predicted by DELPOR. This is at present a defect of our approach. We point out, however, that once the fissuring mechanism begins, the effect of subsequent energy deposition is not very important for the final size of the damage that is simulated. This point of view is supported by our experimental results, which indicate that the size of a crater does not vary with the fluence, provided the threshold has been exceeded. Crater size does, in contrast, depend strongly on the depth of the inclusion.

3 Simulation results

The aim of this work is to simulate the damage produced by a well-defined gold spherical inclusion. As a first step, we studied the damage caused by the laser interaction with a gold sphere of diameter 600 nm embedded in bulk sil-

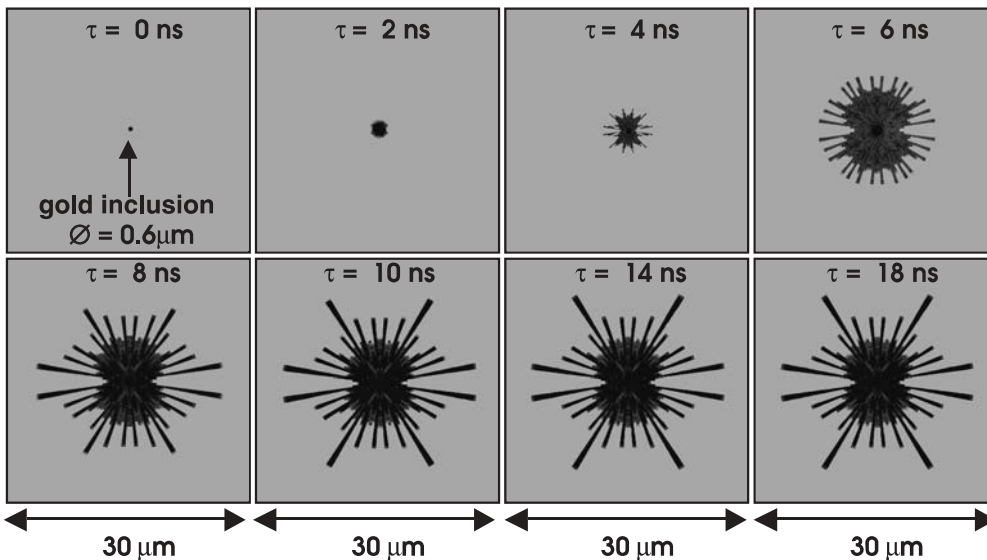


FIGURE 3 Simulation of stresses in bulk silica, at different times, produced by laser irradiation of a gold sphere of radius 600 nm. The fluence is 6 J/cm^2 , the wavelength 355 nm and the pulse duration 3 ns FWHM

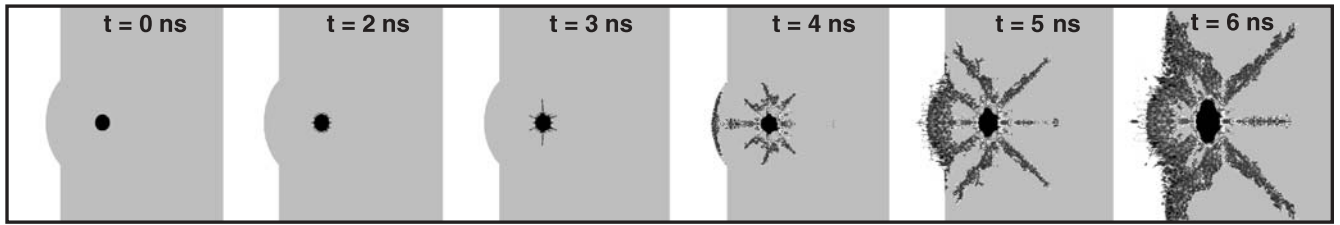


FIGURE 4 Simulation of the fracture propagation produced by irradiation of the gold inclusion located near a free surface, at different times following the arrival of the laser pulse. The fluence is 6 J/cm^2 , the wavelength 355 nm and the pulse duration 3 ns FWHM

ica. We found that, in this case, the size of the damage depends on the laser fluence, but does not grow indefinitely in time. To illustrate this we display in Fig. 3 a time sequence of damage at a fluence of 6 J/cm^2 and a wavelength of 355 nm , which shows that the growth of damage decreases after 8 ns and ceases after 14 ns . The reason for this cessation is that the expanding spherical shock wave is sufficiently attenuated (by distance and damping) that the stress falls below the fracture limit. In this figure the lines of fracture are clearly illustrated, but it should be kept in mind that cylindrical symmetry is assumed, and lines are really cones. In order to simulate real damage to the optical surfaces, the inclusion should be placed somewhere near the surface.

In Fig. 4 we present the results of a simulation of the effects produced by irradiating the configuration shown in Fig. 1b with a laser pulse of fluence 6 J/cm^2 and a wavelength of 355 nm . The fracture lines are shown at several times t since the beginning of the pulse. Since the code assumes axial symmetry, the results shown concern a section through the damaged zone. At $t = 2 \text{ ns}$, the expansion of the heated and compressed particle induces radial fractures in the brittle material. At $t = 4 \text{ ns}$, when the laser intensity is close to its maximum value, these fracture surfaces have grown considerably. In fact, the crossing of the shock wave reflected from the surface with that coming from the inclusion increases the tensile stresses, which lead to the failure of the silica (the dynamic tensile strength is estimated at 0.5 GPa and 3 GPa is the dynamic compressive strength [28]). At the end of the calcu-

lation ($t = 6 \text{ ns}$), the heavily damaged zone is represented by a crater of diameter $8 \mu\text{m}$, from which matter may be ejected. Thus we see that in contrast to the inclusions in bulk (Fig. 3) the inclusions near a surface can produce considerable damage in the form of craters on the surface.

4 Experimental results and comparison with numerical simulations

All the samples we used were prepared by the Laboratoires d'Electronique de Technologie et Instrumentation of the CEA. The parameters and geometry of our samples along with a detailed description of their preparation are given in [29]. Prior to tests of laser damage resistance, the samples were characterized with optical microscopy and atomic force microscopy (AFM) measurements in order to define the nanoparticle size [30]. In Fig. 5a we show one such observation, for a sample where the thickness of the upper coating is $2 \mu\text{m}$. The left-hand part of this figure depicts a Nomarski microscope image, which clearly shows the dome rising above the inclusion. This observation gives us the capability to detect the particle's position before the irradiation. An AFM scan of a small square of the surface around this dome is shown at the center of the figure. To the right of the scan, the height of the dome as a function of distance along the horizontal line is displayed. Note that while the height of the dome corresponds roughly to the diameter of the inclusion (550 nm for this example), the width is much greater. In fact, it depends on the thickness of the outer silica film.

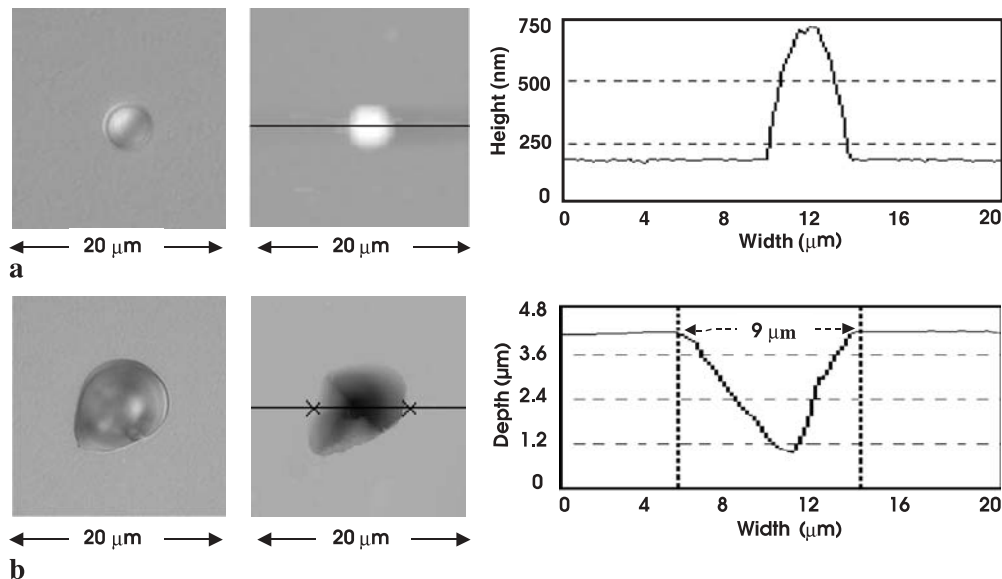


FIGURE 5 Nomarski microscope image and AFM scan of the same surface of our $2\text{-}\mu\text{m}$ -thick upper film sample, showing **a** the dome situated above a gold inclusion and **b** the crater formation after irradiation. Plots of vertical heights vs. horizontal distances show dome and crater profiles

Our samples were irradiated at $\lambda = 355$ nm [31]. The laser spot size was about $9 \mu\text{m}$ at $1/e^2$, so that it was possible to illuminate domes individually. The facility was equipped with an optical microscope, which enabled us to point the laser accurately onto the desired dome. It was thus possible to select different dome sizes, thereby reducing the dispersion in the size of the inclusions. Since the target dome can be chosen sufficiently far from its neighbors, collective effects are thereby avoided. In Fig. 5b we show a Nomarski micrograph of a damage site, together with an AFM scan of the same site. This typical damage results from an inclusion, again embedded at a depth of $2 \mu\text{m}$, irradiated with a single laser shot at a fluence of 6 J/cm^2 . To the right of the scan, the graph presents vertical depth along the horizontal line shown in the AFM image. We see that the generic form of the crater appears to be a cone with a depth of $3.1 \mu\text{m}$ for a width of $9 \mu\text{m}$.

To be able to compare experiment with simulations, we have to determine experimentally the threshold for producing craters. To do this we have performed a statistical analysis of distinct nanoparticle sites, where the thickness of the upper coating is $2 \mu\text{m}$, irradiated with different laser fluences (30 sites per fluence) at wavelength 355 nm. The first crater threshold, defined as the intensity that produces at least one crater when 30 identified inclusion sites are irradiated, is found to be $0.8 \pm 0.1 \text{ J/cm}^2$. The deterministic aspect of our simulations is difficult to compare with this value, given the random nature of the damage phenomena. Therefore, we define another threshold: the intensity needed to obtain craters on half of the irradiated sites. We found this threshold to be $1.5 \pm 0.2 \text{ J/cm}^2$. This is somewhat greater (but of the same order of magnitude) than the value of 1.3 J/cm^2 predicted by the simulations to be the fluence at which crater formation occurs. In general, we can claim that our simulations are in reasonable agreement with the threshold defined above,

At sufficiently large fluence (above 4 J/cm^2) craters are always observed on a given inclusion site. In this situation the use of the 2-D code allows us to predict the size of craters, which may then be compared to the measured sizes. Figure 6

shows comparisons of simulated and observed crater profiles for $2\text{-}\mu\text{m}$ depth of the inclusion. The laser fluence was 6 J/cm^2 at the wavelength of 355 nm. In the upper part of the figure, the profile of the dome (on a section passing through its center), as measured by AFM, is shown on the left, and the corresponding initial condition for the simulation is indicated on the right. The lower part of the figure shows an AFM profile of the crater on the left (passing through the deepest point of the crater) and the predicted crater shape on the right. In fact, the simulation indicates the vertical velocity field of the material that will be ejected to form the crater. For this inclusion depth there is a good agreement between simulated and observed values of the widths and depths of the craters.

5 Conclusion

Previous work has shown that the use of engineered defects of known size, shape and composition is well suited for investigating laser-induced damage in silica. In the present work we used numerical simulations to describe more precisely damages resulting from the interaction of an UV laser with spherical gold inclusions. We have developed a 1-D hydrodynamic code (called DELPOR) to take into account numerous phenomena which occur in the particle and the surrounding silica (laser energy deposition, breakdown, shock waves). In particular, the deposit of energy by the laser is treated following the theory of Mie applied to a medium, which is radially heterogeneous. However, the phenomenon of fracture is not adequately represented by a 1-D spherically symmetric model, and we also use a 2-D Lagrange–Euler hydrodynamics code (called HESIONE). It has been modified to include models for crack initiation and growth, and the 2-D simulations emphasize the importance of the air–glass interface for the formation of craters. The 1-D simulation is used to calculate the energy deposited in the inclusion, which is then used as input to the 2-D code.

Since agreement between numerical and experimental results, obtained on spherical gold inclusions of diameter 600 nm, is relatively good, we claim to have validated our modeling approach. Although these spheres are certainly much larger than the sort of defect that occurs naturally in optical glass, they have the advantage that the individual inclusion sites can be found prior to laser irradiation. It is then straightforward to illuminate them one at a time, observing the resulting damage directly after each shot and to avoid collective effects between two or more inclusions. If the fluence is high enough, we show that when the inclusion is near the surface of the sample damage occurs in the form of crater formation on the surface. Although the 2-D Lagrange–Euler hydrodynamics code HESIONE is not capable of providing a complete description of the morphology of the craters we observe (since 3-D effects are sometimes visible), it does furnish an adequate description of their widths and depths.

The perspectives for continuing this work may proceed in the directions of improvement of the damage-process modeling and refining the experimental approaches. For the simulations, since the large spheres have permitted us to validate the codes, the aim is to correctly simulate successively smaller inclusion until ‘realistic’ nanometric-sized defects can be adequately treated. We point out that preceding work with smaller

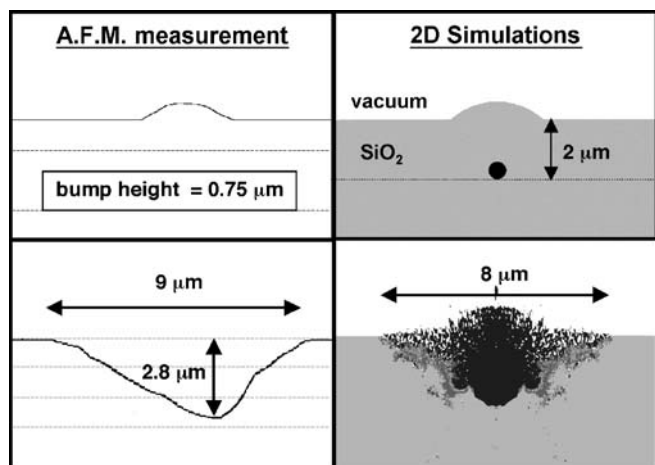


FIGURE 6 Comparison of AFM measurements and code HESIONE simulations for an inclusion at depth $2 \mu\text{m}$. The *upper part* shows the initial configuration, while the *lower part* corresponds to damage produced by laser irradiation (6 J/cm^2 , 355 nm). The simulation indicates the vertical velocity field a few ns after the end of the pulse

gold nanoparticles [8, 10, 11] indicates that the absorptivity of the silica surrounding the inclusion increases and contributes to the total absorption of laser energy. To take this into account, a description of the increase of absorptivity during the irradiation is being introduced in DELPOR. On the experimental side, with the aim of retaining the advantages of using large inclusions, but still approaching smaller sizes of greater empirical interest, we plan to use silica samples with embedded gold spheres of about 50–100-nm diameter.

REFERENCES

- 1 'Laser Induced Damage in Optical Materials: Collected Papers, 1969–1998'. In: *Proc. Boulder Damage Symp.* (SPIE, Bellingham, Washinton, USA 1999)
- 2 N. Bloembergen: *Appl. Opt.* **12**, 661 (1973)
- 3 A. Manenkov, A. Prokhorov: *Sov. Phys. Usp.* **29**, 104 (1986)
- 4 P.P. Hel, D.F. Edwards: *Appl. Opt.* **26**, 4677 (1987)
- 5 J.O. Porteus, F.C. Seitel: *Appl. Opt.* **23**, 3796 (1984)
- 6 R.M. O'Connell: *Appl. Opt.* **31**, 4143 (1992)
- 7 H. Bercegol: *SPIE Proc.* **3902**, 339 (2000)
- 8 S. Papernov, A.W. Schmid, R. Krishnan, L. Tsybeskov: *SPIE Proc.* **4347**, 146 (2001)
- 9 A.V. Hamza, W.J. Siekhaus, A.M. Rubenchik, M.D. Feit, L.L. Chase, M. Savina, M.J. Pellin, I.D. Hutcheon, M.C. Nostrand, M. Runkel, B.W. Choi, M.C. Staggs, M.J. Fluss: *SPIE Proc.* **4679**, 96 (2002)
- 10 S. Papernov, A.W. Schmid: *J. Appl. Phys.* **92**, 5720 (2002)
- 11 F. Bonneau, P. Combis, J.L. Rullier, J. Vierne, M.J. Pellin, M. Savina, M. Broyer, E. Cottancin, J. Tuillon, M. Pellarin, L. Gallais, J.Y. Natoli, M. Perra, H. Bercegol, L. Lamaignère, M. Loiseau, J.T. Donohue: *Appl. Phys. B* **75**, 803 (2002)
- 12 P. Grua, J.P. Morreeuw, H. Bercegol, G. Jonusauskas, F. Vallée: *Phys. Rev. B* **68**, 35424 (2003)
- 13 S. Papernov, A.W. Schmid: *J. Appl. Phys.* **82**, 5422 (1997)
- 14 P. Combis, F. Bonneau, G. Daval, L. Lamaignère: *SPIE Proc.* **3902**, 317 (2000)
- 15 G. Mie: *Ann. Phys. (4)* **25**, 377 (1908)
- 16 M. Born, E. Wolf: *Principles of Optics* (Pergamon, Oxford 1980) Chapt. 13
- 17 F. Bonneau, P. Combis, J. Vierne, G. Daval: *SPIE Proc.* **4347**, 308 (2001)
- 18 F. Bonneau, P. Combis, J.B. Gaudry, G. Daval: *SPIE Proc.* **4347**, 560 (2001)
- 19 F. Bonneau, B. Cazalis: *SPIE Proc.* **2714**, 650 (1996)
- 20 A.V. Bushman, I.V. Lomonosov, V.E. Fortov: *Sov. Tech. Rev. B* **5**, 1 (1993)
- 21 E. Palik: *Handbook of Optical Constants of Solids* (Academic, London 1985)
- 22 W. Ebeling, A. Förster, V. Fortov, V. Griaznov, A. Polishchuk: *Thermophysical Properties of Hot Dense Plasmas* (Teubner, Stuttgart 1991)
- 23 A. Decoster, P. Markowich, B. Perthame: *Modeling of Collisions* (Gauthier-Villars, Paris 1998)
- 24 D. Arnold, E. Cartier: *Phys. Rev. B* **46**, 15102 (1992)
- 25 L.V. Keldysh: *Sov. Phys. JETP* **20**, 1307 (1965)
- 26 M.B. Rubin, A.V. Attia: LLNL UCRL ID 104759 (1990)
- 27 J.M. Chevalier, I. Bertron, F. Malaise, R. Courchinoux: in *Proc. 53rd Meet. Aeroballistic Range Association, 2002*
- 28 D.R. Faux: LLNL UCRL ID 128520 (1997)
- 29 F. Bonneau, P. Combis, J.L. Rullier, J. Vierne, H. Ward, H. Bercegol, P. Bouchut, J. Donohue, L. Gallais, L. Lamaignère, C. Le Diraison, M. Loiseau, J.Y. Natoli, C. Pellé, M. Perra: *SPIE Proc.* **4760**, 1055 (2002)
- 30 J.Y. Natoli, P. Volto, M. Pommies, G. Albrand, C. Amra: *SPIE Proc.* **3244**, 76 (1998)
- 31 L. Gallais, J.Y. Natoli: *Appl. Opt.* **42**, 960 (2003)